Ground-state tuning of metal-insulator transition by compositional variations in $BaIr_{1-x}Ru_xO_3$ ($0 \leqslant x \leqslant 1$)

S. J. Yuan,[1,*] K. Butrouna,[1] J. Terzic,[1] H. Zheng,[1] S. Aswartham,[1] L. E. DeLong,[1] Feng Ye,[2] P. Schlottmann,[3] and G. Cao[1,†]

[1]*Department of Physics and Astronomy, Center for Advanced Materials, University of Kentucky, Lexington, Kentucky 40506, USA*

[2]*Quantum Condensed Matter Division, Oak Ridge National Laboratory, Oak Ridge, Tennessee 37831, USA*

[3]*Department of Physics, Florida State University, Tallahassee, Florida 32306, USA*

(Received 9 October 2015; revised manuscript received 23 March 2016; published 25 April 2016)

Hexagonal $BaIrO_3$ is a magnetic insulator driven by the spin-orbit interaction (SOI), whereas $BaRuO_3$ is an enhanced paramagnetic metal. Our investigation of structural, magnetic, transport, and thermal properties reveals that substitution of Ru^{4+} ($4d^4$) ions for Ir^{4+} ($5d^5$) ions in $BaIrO_3$ reduces the magnitudes of the SOI and a monoclinic structural distortion and rebalances the competition between the SOI and the lattice degrees of freedom to render an evolution from a magnetic insulting state to a robust metallic state. The central findings of this paper are as follows: (1) light Ru doping ($0 < x \leqslant 0.15$) prompts simultaneous, precipitous drops in both the magnetic ordering temperature T_N and the electrical resistivity, and (2) heavier Ru doping ($0.41 \leqslant x \leqslant 0.9$) induces a robust metallic state without any long-range magnetic order. All results suggest a critical role of the lattice degrees of freedom in determining the ground state in the heavy transition-metal oxides.

DOI: 10.1103/PhysRevB.93.165136

I. INTRODUCTION

A unique feature of the $5d$ iridates is that a strong spin-orbit interaction (SOI) competes vigorously with Coulomb interactions, noncubic crystalline electric fields, and Hund's rule coupling [1–5]. The relative strengths of these interactions stabilize new exotic ground states that provide a fertile ground for studying new physics. In particular, it is now recognized that strong SOI can drive novel narrow-gap Mott insulating states in iridates. The SOI is a relativistic effect that is proportional to Z^2 (Z is the atomic number), is approximately 0.4 eV in the iridates (compared to ~20 meV in $3d$ materials), and splits the t_{2g} bands into states with $J_{\text{eff}} = 1/2$ and $J_{\text{eff}} = 3/2$, the latter having lower energy. Since the Ir^{4+} ($5d^5$) ions provide five $5d$ valence electrons, four of them fill the lower $J_{\text{eff}} = 3/2$ bands, and one electron partially occupies the $J_{\text{eff}} = 1/2$ band in which the Fermi level E_F resides. The $J_{\text{eff}} = 1/2$ band is so narrow that even a reduced U (~0.50 eV due to the extended nature of $5d$-electron orbitals) is sufficient to open a gap ($\leqslant$0.62 eV) that induces a novel insulating state, which is contrary to expectations based upon the relatively large unsplit $5d$ bandwidth [1–3,6].

Adopting a distorted hexagonal structure with both face-sharing and corner-sharing IrO_6 octahedra, $BaIrO_3$ is particularly unique in that it exhibits a simultaneous onset of weak ferromagnetic transition due to a canted antiferromagnetic structure and charge-density wave (CDW) orders with Néel temperature $T_N = 183$ K, comparable to that of other iridates, such as 240 K for Sr_2IrO_4 [7] and 285 K for $Sr_3Ir_2O_7$ [8], and a temperature-driven transition from a bad metal to an insulating ground state [9–11]. The ground state of $BaIrO_3$ is extremely sensitive to lattice contractions that can be tuned by light doping or the application of hydrostatic pressures [4,12,13]. The extraordinary delicacy of the ground state in $BaIrO_3$ implies a critical balance among orbital, electronic, and lattice degrees of freedom [4,14]. The hexagonal structure of $BaIrO_3$ is similar to that of nine-layered rhombohedral $BaRuO_3$, which exhibits a crossover from metallic to insulating behavior and enhanced paramagnetism with decreasing temperature [15,16]. However, a monoclinic distortion extant in $BaIrO_3$ at room temperature and 90 K generates twisting and buckling of the cluster trimers (see Fig. 1) that give rise to two one-dimensional (1D) zigzag chains along the c axis and a two-dimensional layer of corner-sharing IrO_6 octahedra on the ab plane [9,12,17–19].

Although $BaIrO_3$ and $BaRuO_3$ have similar structures, they exhibit sharply contrasting physical properties, which underscore the critical role SOI (~0.4 eV for iridates and ~0.15 eV for ruthenates) [3], and the lattice degrees of freedom can play in determining the ground state in iridates. In this paper, substituting Ru^{4+} ($4d^4$) for Ir^{4+} ($5d^5$) in single-crystal $BaIr_{1-x}Ru_xO_3$($0 \leqslant x \leqslant 1$) reduces the magnitude of the SOI, the structural distortions, and adds holes to the t_{2g} bands. The overall effect of Ru doping is to lower E_F and move the system away from the Mott instability toward a more robust metallic state. The emerging metallic state with delocalized electrons also accompanies a decrease in T_N.

II. EXPERIMENT

The single crystals of $BaIr_{1-x}Ru_xO_3$ were grown by conventional flux methods similar to earlier reports [9,15] using $BaCl_2$ as a self-flux. Crystals were grown in platinum crucibles using IrO_2 (99.98%, Alfa Aesar), RuO_2 (99.98%, Alfa Aesar), $BaCO_3$ (99.99%, Alfa Aesar), and anhydrous $BaCl_2$ (99.5%, Alfa Aesar). Starting powders were placed in a Pt crucible with a Pt lid, and this assembly was then put in an alumina crucible with a cover. The mixtures were heated up to 1480 °C and then cooled to 1350 °C at a rate of 5 °C per hour before cooling down to room temperature. The ratio of the sample to flux remains at 1:8 throughout the entire series of $BaIr_{1-x}Ru_xO_3$. The crystals have a hexagonal surface and a visible layered texture along the c axis as

*Corresponding author: sjyuan.shu@gmail.com

†cao@uky.edu

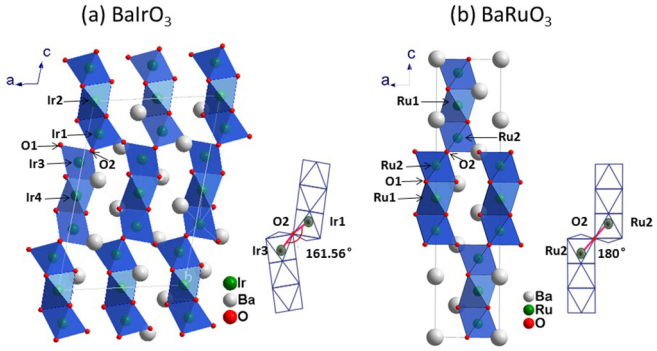

FIG. 1. Comparison of the nine-layer crystallographic form (a) $BaIrO_3$ and (b) $BaRuO_3$ crystal structure. Note the corner-sharing Ir_3O_{12} and Ru_3O_{12} trimers that are connected through the vertices of the top and bottom octahedra of the trimers and the schematic of the M-O_2-M bond angle θ (M = Ir or Ru).

shown in the inset of Fig. 2(a). The crystal structures were determined using a Nonius Kappa CCD x-ray diffractometer or a Rigaku x-ray diffractometer XtaLAB PRO equipped with a PILATUS 200-K hybrid pixel array detector at 90 or 240 K, and they were refined by full matrix least squares using the SHELX-97 programs [20]. The standard deviations of all lattice parameters and interatomic distances are smaller than 0.1%. The atomic parameters for $BaIr_{1-x}Ru_xO_3$ are available in the Supplemental Material [21]. Chemical compositions of the single crystals were estimated using a combined unit of

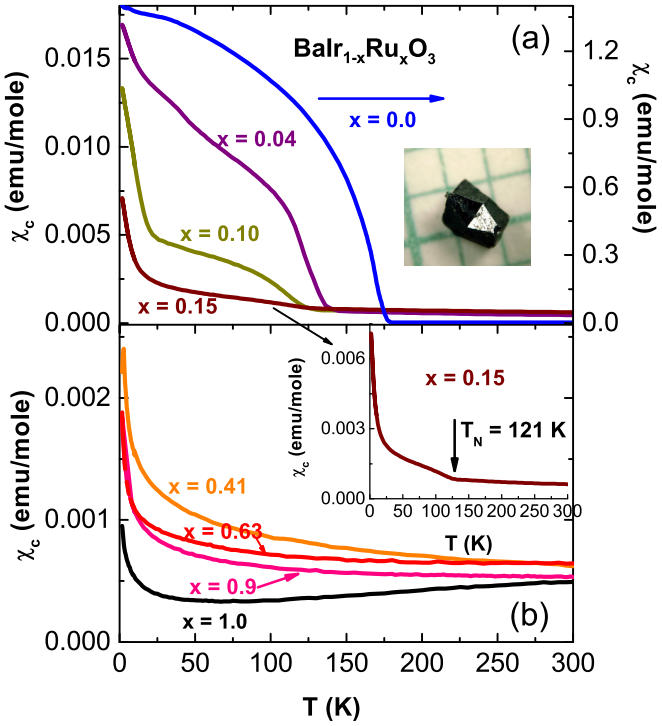

FIG. 2. The magnetic susceptibilities $\chi(T)$ along the c axis for $BaIr_{1-x}Ru_xO_3$ where (a) $0 \leqslant x \leqslant 0.15$ and (b) $0.42 \leqslant x \leqslant 1$. The data were collected after a field cooling procedure at $\mu_0 H = 0.1$ T. The inset in (a) shows a representative single crystal of $BaIr_{1-x}Ru_xO_3$ with $x = 0$. The inset in (b) shows an enlarged $\chi_c(T)$ for $x = 0.15$.

Hitachi/Oxford SwiftED 3000 for energy dispersive x-ray spectroscopy. The magnetization $M(T)$, electrical resistivity $\rho(T)$, and specific heat $C(T)$ were measured between 1.7 and 400 K using a Quantum Design 7T superconducting quantum interference device (SQUID) magnetometer and a Quantum Design 9T physical property measurement system, respectively.

III. RESULTS AND DISCUSSION

The two end members $BaIrO_3$ and $BaRuO_3$ both have nine-layer rhombohedral phases with different space groups as shown in Figs. 1(a) and 1(b). The $C2/m(12)$ space group of $BaIrO_3$ features three face-sharing IrO_6 octahedra forming Ir_3O_{12} trimers that are corner and face shared via IrO_6 octahedra (containing Ir_1 and Ir_3 sites) to form 1D chains along the c axis [12,16–19] [see Fig. 1(a)]. A monoclinic distortion generates twisting and buckling of the trimers (tilted $\sim 12^\circ$ relative to each other), which gives rise to two 1D zigzag chains along the c axis and a two-dimensional layer of corner-sharing IrO_6 octahedra on the ab plane. Substituting Ru^{4+} for Ir^{4+} preserves the monoclinic structure in the entire doping range ($x \leqslant 0.90$) except for $x = 1$ as shown in Table I. It results in a nearly uniform reduction in lattice parameters a-c axes and the unit-cell volume V. This behavior is expected because the ionic radius of Ru^{4+} (0.620 Å) is slightly smaller than that of Ir^{4+} (0.625 Å). In addition, the Ir/Ru-O-Ir/Ru bond angle θ increases linearly with increasing Ru concentration x and eventually reaches 180° for $x = 1$ (i.e., $BaRuO_3$), indicating a significantly less distorted lattice. $BaRuO_3$ or $x = 1$ exhibits a similar crystal structure with the $R\bar{3}m$ (166) space group as shown in Fig. 1(b). Three RuO_6 octahedra share faces in a partial chain, facilitating direct Ru-Ru d-orbital interactions between the octahedra. Each of these triple units or trimers of the octahedra shares corners with its neighbors along the hexagonal axis via nearly 180° bond angles that favor superexchange coupling [Fig. 1(b)].

Ru doping induces pronounced changes in a wide range of physical properties of single-crystal $BaIr_{1-x}Ru_xO_3$. Representative data for the c-axis magnetic susceptibility $\chi_c(T)$ that shows the weak magnetic transition at T_N is depressed from 183 K for $x = 0$ to 145 K for $x = 0.04$ and vanishes for $x \geqslant 0.41$ is presented in Fig. 2.

The magnetic anisotropy also decreases with Ru additions as shown in Fig. 3. Magnetic anisotropy is in general a result of SOI; Ru doping weakens the SOI, therefore, leading to a smaller magnetic anisotropy. Furthermore, Hund's rule coupling competes with the SOI and thus weakens the relative strength of the SOI. With increasing x, the c-axis susceptibility $\chi_c(T)$ becomes relatively stronger and larger than the basal-plane susceptibility $\chi_{ab}(T)$ [see Figs. 3(b) and 3(c)]. This change suggests a spin flop from the basal plane to the c axis due to Ru doping. For $x = 1$, the basal-plane $\chi_{ab}(T)$ is larger than $\chi_c(T)$ again [see Fig. 3(d)]. Similar phenomena were also observed in $Ca_2Ru_{1-x}Ir_xO_4$ [22] and $Sr_2Ir_{1-x}Ru_xO_4$ [23]. This behavior could be due to the strong interaction between Ru $4d$ and Ir $5d$ electrons.

It is already established that the bond angle θ is critical to the electronic and magnetic structures of iridates [4]. As shown in Fig. 4(a), θ increases linearly with increasing x and

TABLE I. The crystal structure and refinement details of $BaIr_{1-x}Ru_xO_3$ at 90 K for $x = 0$, 0.10, 0.63, and 1 and at 240 K for $x = 0.82$ and 0.90. The diffracometer is a Nonius Kappa CCD, and the aborption correction is a multiscan SADABS. The Ir/Ru-O_2-Ir/Ru bond angle is defined in Fig. 1.

	$x = 0$ (90 K)	$x = 0.10$ (90 K)	$x = 0.63$ (90 K)	$x = 0.82$ (240 K)	$x = 0.90$ (240 K)	$x = 1$ (90 K)
			Crystal data			
Crystal system, space group	Monoclinic, $C12/m1(12)$	Monoclinic, $C12/m1(12)$	Monoclinic, $C12/m1(12)$	Monoclinic, $C12/m1(12)$	Monoclinic, $C12/m1(12)$	Trigonal, $R\bar{3}m$ (166)
a-c (Å)	$a = 9.9935(2)$, $b = 5.7352(1)$, $c = 15.2376(3)$	$a = 9.9839(2)$, $b = 5.7377(1)$, $c = 15.1107(4)$	$a = 9.9440(2)$, $b = 5.7429(1)$, $c = 14.8102(4)$	$a = 9.9999(5)$, $b = 5.7759(4)$, $c = 14.8916(4)$	$a = 9.9923(4)$, $b = 5.7733(3)$, $c = 14.8882(8)$	$a = 5.7366(1)$, $c = 21.5933(6)$
β (deg)	103.411(1)	103.3402(9)	102.8574(9)	102.939(5)	102.882(4)	NA
V (Å^3)	849.10(6)	842.25(3)	824.57(3)	838.28(8)	837.26(7)	615.40(3)
Z	12	12	12	12	12	9
Bond angle (deg)	161.671(1)	163.678(0)	174.296(1)	175.1(3)	176.1(1)	180.0
			Data collection			
Number of measured, independent, and observed $[I > 4\sigma(I)]$ reflections	6066,398,350	7075,396,369	7210,398,353	14459,1643,1525	14071,1769,1633	7256,401,398
Rint	0.021	0.031	0.035	0.027	0.038	0.025
			Refinement			
$R[F^2 > 4\sigma(F^2)]$, $wR(F^2)$, S	0.016,0.035,1.05	0.02,0.049,1.15	0.025,0.069,1.17	0.067,0.1847,1.085	0.0720.205,1.024	0.02,0.035,1.09

eventually reaches an ideal 180° for $x = 1$. The increase in θ directly enhances the electron hopping and favors a more metallic state with a concurrent decrease in T_N [see Fig. 4(b)].

Indeed, the evolution from the insulating to the itinerant state upon Ru doping is clearly illustrated in the electrical resistivity $\rho(T)$. For $x = 0$, both the ab plane and the c axis $\rho_{ab}(T)$ and $\rho_c(T)$ exhibit a sharp kink at $T_N = 183$ K, consistent with previous results in which the energy gap is estimated to be 0.1 eV [9,17]. With Ru doping, both $\rho_{ab}(T)$ and $\rho_c(T)$ decrease rapidly (see Fig. 5). It is noted that the metallic behavior at higher temperatures for $x = 0.04$ [see Fig. 5(b)] does not seem to follow the general trend displayed by other compositions although the behavior is highly reproducible.

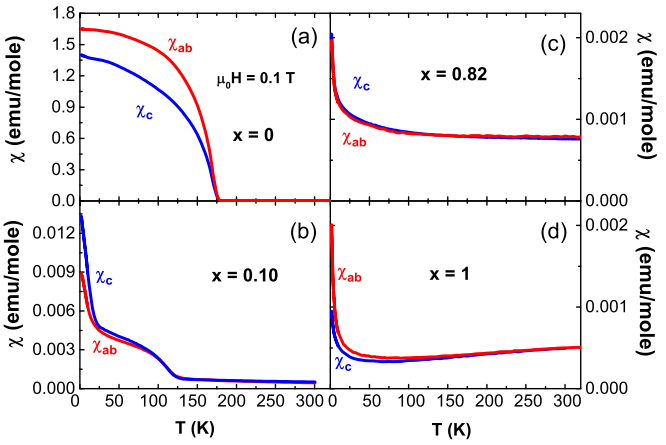

FIG. 3. The magnetic susceptibilities $\chi(T)$ on the ab plane and along the c axis for representative compositions (a) $x = 0$, (b) $x = 0.10$, (c) $x = 0.82$, and (d) $x = 1$, respectively. The magnetization was measured after field cooling at $\mu_0 H = 0.1$ T.

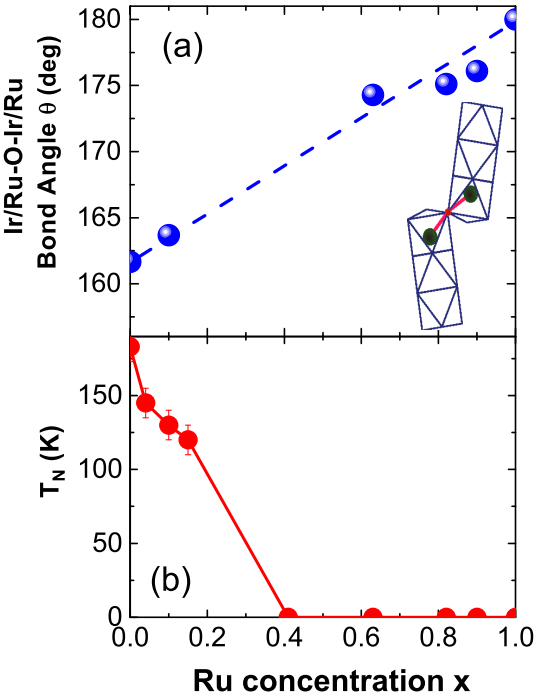

FIG. 4. The Ru concentration x dependence of (a) the Ir/Ru-O_2-Ir/Ru bond angle θ and (b) T_N. The inset: schematic of the Ir/Ru-O_2-Ir/Ru bond angle θ. Note that θ increases linearly with increasing x.

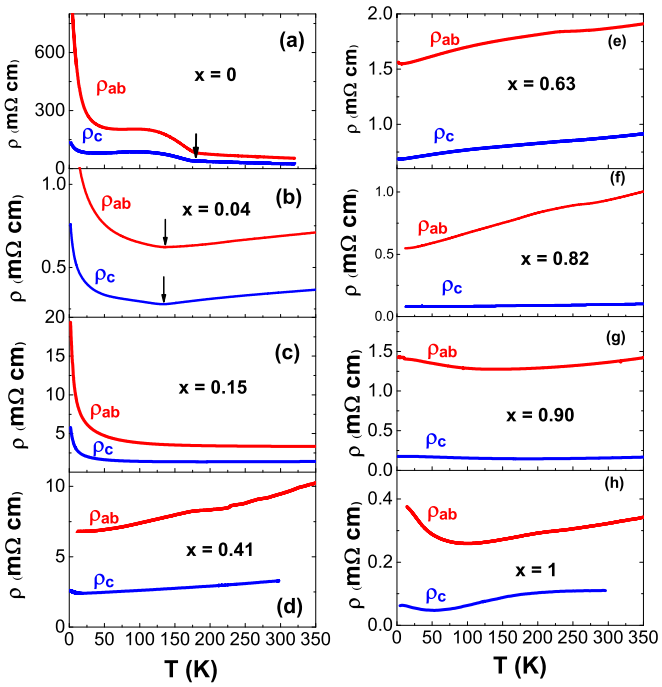

FIG. 5. The temperature dependence of the resistivity $\rho(T)$ for representative compositions (a) $x = 0$, (b) $x = 0.04$, (c) $x = 0.15$, (d) $x = 0.41$, (e) $x = 0.63$, (f) $x = 0.82$, (g) $x = 0.90$, and (h) $x = 1$. The vertical arrows indicate the kink that corresponds to the weak magnetic transition at $T = T_N$.

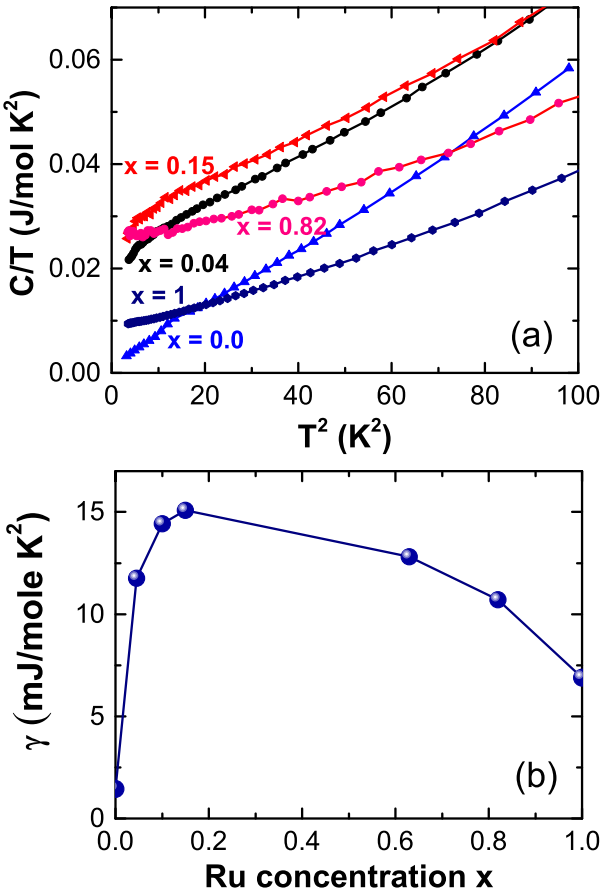

FIG. 6. (a) The specific heat $C(T)/T$ vs T^2 and (b) the Sommerfeld coefficient γ vs x for $BaIr_{1-x}Ru_xO_3$.

The origin of this brief occurrence of the metallic state is yet to be understood. Nevertheless, dilute Ru substitutions for Ir result in a reduced $\rho(T)$ and an emerging metallic state for $x > 0.15$. For $x = 1$ or $BaRuO_3$, a broad upturn in $\rho_{ab}(T)$ at low temperatures might be a result of a pseudogap formation and 1D-CDW fluctuations according to Ref. [16].

The temperature dependence of the specific heat $C(T)$ for various x's is given in Fig. 6(a). Fitting the data to $C(T) = \gamma T + \beta T^3$ for $7 < T < 17$ K yields the Sommerfeld coefficient γ for the electronic contribution to $C(T)$ [see Fig. 6(b)], which serves as a measure of the electronic density of states at the Fermi level $N(E_F)$ and the effective mass of the carriers. There is a substantial increase in γ with dilute Ru concentration; in particular, γ reaches 11.75 mJ mol^{-1} K^{-2} for $x = 0.04$ and 15.09 mJ mol^{-1} K^{-2} for $x = 0.15$, compared to $\gamma = 2.34$ mJ mol^{-1} K^{-2} for the parent compound ($x = 0.0$). The γ for $0.04 \leqslant x \leqslant 0.15$ in which the metallic state is not fully developed is unexpectedly high, and this is likely due to spin fluctuations existent in the system. Nevertheless, $N(E_F)$ and γ eventually decrease with x as shown in Fig. 6(b). In the case of $BaRuO_3$, the smaller values reflect pseudogap formation due to the CDW instability [16].

IV. CONCLUSIONS

We have investigated the structural, magnetic, transport, and thermal properties of $BaIr_{1-x}Ru_xO_3$. Ru doping rebalances the competition among the SOI, electron correlations, and the lattice degrees of freedom to generate a metallic state for $x > 0.15$. The Ru doping alters the relative strength of the SOI that dictates the ground state, which, in turn, affects the band gap near E_F. Unlike the situation in Sr_2IrO_4 that features an unconventional correlation between the magnetic transition and the charge gap, the evolution of the ground state in $BaIr_{1-x}Ru_xO_3$ appears to indicate a strong coupling between the magnetic order and the metal-insulator transition. All results suggest the critical role of lattice degrees of freedom that, along with the SOI, dictate the ground state of the heavy transition-metal oxides.

ACKNOWLEDGMENTS

This work was supported by the National Science Foundation via Grant No. DMR-1265162 (G.C.) and Department of Energy (BES) through Grants No. DE-FG02-98ER45707 (P.S.) and No. DE-FG02-97ER45653 (L.E.D.).

[1] B. J. Kim, H. Jin, S. J. Moon, J. Y. Kim, B. G. Park, C. S. Leem, J. Yu, T. W. Noh, C. Kim, S. J. Oh, J. H. Park, V. Durairaj, G. Cao, and E. Rotenberg, Phys. Rev. Lett. **101**, 076402 (2008).

[2] B. J. Kim, H. Ohsumi, T. Komesu, S. Sakai, T. Morita, H. Takagi, and T. Arima, Science **323**, 1329 (2009).
[3] G. Cao and L. E. DeLong, in *Frontiers of 4d- and 5d-Transition Metal Oxides* (World Scientific, Singapore, 2013).
[4] O. B. Korneta, S. Chikara, S. Parkin, L. E. DeLong, P. Schlottmann, and G. Cao, Phys. Rev. B **81**, 045101 (2010).
[5] T. F. Qi, O. B. Korneta, L. Li, K. Butrouna, V. S. Cao, X. Wan, P. Schlottmann, R. K. Kaul, and G. Cao, Phys. Rev. B **86**, 125105 (2012).
[6] J. Dai, E. Calleja, G. Cao, and K. McElroy, Phys. Rev. B **90**, 041102 (2014).
[7] G. Cao, J. Bolivar, S. McCall, J. E. Crow, and R. P. Guertin, Phys. Rev. B **57**, R11039 (1998).
[8] G. Cao, Y. Xin, C. S. Alexander, J. E. Crow, P. Schlottmann, M. K. Crawford, R. L. Harlow, and W. Marshall, Phys. Rev. B **66**, 214412 (2002).
[9] G. Cao, J. E. Crow, R. P. Guertin, P. F. Henning, C. C. Homes, M. Strongin, D. N. Basov, and E. Lochner, Solid State Commun. **113**, 657 (2000).
[10] M. L. Brooks, S. J. Blundell, T. Lancaster, W. Hayes, F. L. Pratt, P. P. C. Frampton, and P. D. Battle, Phys. Rev. B **71**, 220411 (2005).
[11] M. A. Laguna-Marco, D. Haskel, N. Souza-Neto, J. C. Lang, V. V. Krishnamurthy, S. Chikara, G. Cao, and M. van Veenendaal, Phys. Rev. Lett. **105**, 216407 (2010).
[12] G. Cao, X. N. Lin, S. Chikara, V. Durairaj, and E. Elhami, Phys. Rev. B **69**, 174418 (2004).
[13] M. A. Laguna-Marco, G. Fabbris, N. M. Souza-Neto, S. Chikara, J. S. Schilling, G. Cao, and D. Haskel, Phys. Rev. B **90**, 014419 (2014).
[14] W. Ju, G.-Q. Liu, and Z. Yang, Phys. Rev. B **87**, 075112 (2013).
[15] M. Shepard, S. McCall, G. Cao, and J. E. Crow, J. Appl. Phys. **81**, 4978 (1997).
[16] Y. S. Lee, J. S. Lee, K. W. Kim, T. W. Noh, J. Yu, Y. Bang, M. K. Lee, and C. B. Eom, Phys. Rev. B **64**, 165109 (2001).
[17] A. V. Powell and P. D. Battle, J. Alloys Compd. **191**, 313 (1993).
[18] M. H. Whangbo and H. J. Koo, Solid State Commun. **118**, 491 (2001).
[19] R. Lindsay, W. Strange, B. L. Chamberland, and R. O. Moyer, Jr., Solid State Commun. **86**, 759 (1993).
[20] G. M. Sheldrick, Acta Cryst. **A64**, 112 (2008).
[21] See Supplemental Material at http://link.aps.org/supplemental/10.1103/PhysRevB.93.165136 for substantial information on crystal refinements.
[22] S. J. Yuan, J. Terzic, J. C. Wang, L. Li, S. Aswartham, W. H. Song, F. Ye, and G. Cao, Phys. Rev. B **92**, 024425 (2015).
[23] S. J. Yuan, S. Aswartham, J. Terzic, H. Zheng, H. D. Zhao, P. Schlottmann, and G. Cao, Phys. Rev. B **92**, 245103 (2015).